Fennoscandian strain rates from BIFROST GPS: A gravitating, thick-plate approach

H.-G. Scherneck [a,*], M. Lidberg [b], R. Haas [a], Jan M. Johansson [a], G.A. Milne [c]

[a] *Chalmers University of Technology, Dept. of Radio and Space Science, SE-412 96 Göteborg, Sweden*
[b] *National Land Survey of Sweden, SE-801 82 Gävle, Sweden*
[c] *University of Ottawa, Dept. of Geosciences, Ottawa, Ont., Canada*

ARTICLE INFO

ABSTRACT

The aim of this investigation is to develop a method for the analysis of crustal strain determined by station networks that continuously measurements of Global Navigation Satellite Systems (GNSS). The major new ingredient is that we require a simultaneous minimum of the observation error and the elastic and potential energy implied by the deformation.

The observations that we analyse come from eight years worth of daily solutions from continuous BIFROST GPS measurements in the permanent networks of the Nordic countries and their neighbours. Reducing the observations with best fitting predictions for the effects of glacial isostatic adjustment (GIA) we find strain rates of maximum 5 nano/yr in the interior of the rebound area predominantly as areal strain. The largest strain rates are found in the Finnmarken area, where however the GNSS network density is much lower than in the central and southern parts.

The thick-plate adjustment furnishes a simultaneous treatment of 3-D displacements and the ensuing elastic and potential energy due to the deformation. We find that the strain generated by flexure due to GIA is important. The extensional regime seen at the surface turns over into a compressive style already at moderated depth, some 50 km.

© 2009 Elsevier Ltd. All rights reserved.

1. Introduction

In application to contemporary deformation observed with space geodetic techniques, the computation of strain rates has so far mostly been done on the basis of kinematic and/or stochastic concepts, and the potential importance the vertical motion component has been mentioned in only in passing (Cai and Grafarend, 2007). The majority of earlier studies has concentrated on strain accumulation at fault zones (e.g. Spakman and Nyst (2002); Nyst and Thatcher (2004)) in problems dominated by horizontal motion.

The situation in the area of glacial isostatic adjustment (GIA) for instance in Fennoscandia differs in many respects. Vertical motion is on the order of 10 mm/yr, almost an order of magnitude greater than the horizontal motion; the field of motion does not appear to be substantially modulated by individual fault zones.

While the method of Spakman and Nyst (2002) produces grids that are rather independent of the network of observing stations, the work of the other authors, including the VLBI results of Haas et al. (2002) and investigations of the ITRF station network by Nocquet et al. (2005) present their strain rates on triangulations directly dependent on the site locations, with the consequence that area is

covered with a highly irregular grid; the strain rates are treated as constants in each triangle. One thought behind the present study is to facilitate interpolation of strain rates on the basis of continuous polynomials, using elasto-mechanical constraints rather than stochastic methods.

Continuous observations from the BIFROST GNSS network in Fennoscandia are available starting in 1993. Recent comparisons of inferred rates of motion with GIA models (Milne et al., 2004; Lidberg et al., 2006, 2010) suggest that the observations can successfully be reconciled at a level of 5 of the weighted χ^2 of fit. This leaves little signal for further investigation of systematic deficiencies of the model or systematic errors in the estimated station velocities. Nevertheless this paper will pursue an attempt to determine areas where the misfit might show patterns pertaining over scales wider than the local site scale.

The following concept is employed. The elastic equations for a thick plate are formulated. We take into account that the plate is part of a spherical shell. The plate is streched and flexed such that the station velocities are matched, minimising a cost function in an overdetermined system of observation equations. Free slip boundary conditions allow the plate a maximum degree of freedom. Vertical strain is neglected. The cost of deformation comprises elastic and potential energy, and the observation misfit. Strain and curl rates result as derivate products. The relation between a measure of elastic energy and the velocity field will be addressed.

---

* Corresponding author.
  E-mail address: hgs@chalmers.se (H.-G. Scherneck).

In one view the thick-plate adjustment may just serve as an interpolation method for site velocities. This would correspond to a conservative attitude, being cautious as to some of the basic assumptions like free slip boundary conditions and homogeneous slab. The diametrical view, expecting the model's 3-D deformation to be sufficiently consistent with an elastic lithosphere, is probably over-optimistic. One virtue of the approach might be seen in its independence of a GIA assumption. We employ this notion at the stage where we analyse that part of the GNSS observations that deviates from a best fitting model for GIA.

2. Model

We define a penalty function consisting of the normalised RMS of the misfit of the 3-D motion, elastic energy and gravitational energy. The elastic energy comprises in-plane and bending stresses and strains. The gravitational energy sums up contributions of the buoyancy of displaced layers. We have taken a small series of density jumps (at surface, crust–mantle, and 700 km boundaries). A scaling factor must be devised that trades off the observation misfit against the energy in the elastic and buoyant features.

The buoyant property has been found important to include. Without it, the model accomplishes heavy warping in areas where measurements are not available.

Stress and strain is formulated in a spherical geometry. The base functions chosen consist of a three-set of 2D Chebyshev polynomials for the observables, the vertical and horizontal displacement rates. The polynomials have the latitude and longitude angles as independent variables. The square interval (lower left and upper right corner) $[(-1, -1), (1, 1)]$ is mapped to a quadrangle containing the area of interest. Strain rate is derived from deformation rate using the appropriate formulas from differential geometry. The effects from bending of the thick plate are formulated using only the leading terms, which are those known from a plane geometry.

The differential operators have been derived using Mathematica with Weisstein (s.d.) as a guideline.

Another derivate useful to consider is local rotation (a.k.a. curl). A spheroidal-modes model of GIA like the one used in Milne et al. (2004) is not capable of producing curl; however a thin or a thick plate is. Thus, significant amounts of curl in the horizontal motion could indicate non-GIA conditions or an impact due to deviations of a radially nonsymmetric earth structure.

2.1. Energy

In the thick-plate adjustment observation error is traded against elastic and potential energy. The rate of energy E that gets stored in a volume dV is computed from the relation

$$\frac{\mathrm{d}E}{\mathrm{d}t}\,\mathrm{d}V = (\mathbf{f}\cdot\dot{\mathbf{u}} + \boldsymbol{\sigma}:\dot{\boldsymbol{\epsilon}})\,\mathrm{d}V$$

In the case of work against the potential we may suppose that force density $\mathbf{f} \propto -\mathbf{u}$,

$$f_r = -g\,\delta\rho\,u_r = -g\,\delta\rho\,\dot{u}_r\,t$$

i.e.

$$\dot{\mathbf{u}} \propto -\mathbf{u}$$

In GIA this relation holds only for a single-mode approximation of the process. A strict, local relation between $\dot{\mathbf{u}}$ and $\mathbf{u}$ would require the introduction of a spatial–temporal filter in order to account for the dispersion of visco-elastic Love-numbers in the wave number-relaxation time space. However, this would still imply the assumption that all motions were excited by glacial loading. In trying to keep the thick-plate model as independent

of GIA-assumptions as possible we rather assume a constant local proportionality. Therefore our buoyancy energy term will only take the product

$$g\frac{t^2}{2}\int \delta\rho\,\dot{\mathbf{u}}\cdot\dot{\mathbf{u}}\ \mathrm{d}V$$

into account, surmising that we minimise the work of a plate as it departs from an undeformed state to the incremental deformation occurring in one unit of time.

Similarly, in the case of elastic energy we ignore the background stress and minimise only the work due to the stress increment of the ongoing deformation. Since the problem involves only a purely elastic plate, the application of the principle of correspondence is trivial.

2.2. Model details

Let R denote the radius of the earth and take a quadrangle of width $\Delta\Lambda$ in longitude and $\Delta\Phi$ in latitude, centred at Λ_0 and Φ_0, encompassing the area of interest. We formulate the 3-D displacements as a finite sum of Chebyshev polynomials

$$\mathbf{u}(\xi, \eta) = \sum_{i=0, j=0}^{N,M} \mathbf{U}_{ij}\ T_i(\xi)\ T_j(\eta) \tag{1}$$

with $\mathbf{u} = [u, v, w]$ vertical, south, east displacement in the mid-plane of a thick elastic slab, $-1 \le \xi \le 1$, $-1 \le \eta \le 1$, longitude $\lambda = \Lambda_0 + \xi\ \Delta\Lambda/2$, and colatitude $\phi = \Phi_0 + \eta\ \Delta\Phi/2$. When we consider a thick plate the displacements in (1) represent the neutral layer, and the displacement along the surface, i.e. the result of bending, must be added.

The thin-plate strain components and rotation ω_z are readily computed from

$$\epsilon_{\phi\phi} = \frac{1}{R}\left(\frac{\partial v}{\partial\phi} + u\right) \tag{2}$$

$$\epsilon_{\lambda\lambda} = \frac{1}{R\sin\phi}\left(\frac{\partial w}{\partial\lambda} + \sin(\phi)u + \cos(\phi)v\right) \tag{3}$$

$$\epsilon_{\phi\lambda} = \frac{1}{2R\sin\phi}\left(\frac{\partial v}{\partial\lambda} + \sin\phi\frac{\partial w}{\partial\phi} - 2\cos(\phi)w\right) \tag{4}$$

$$\omega_z = \frac{1}{2R}\left(\frac{\partial w}{\partial\phi} - \frac{1}{\sin\phi}\frac{\partial v}{\partial\lambda} + \cot(\phi)w\right) \tag{5}$$

and

$$\frac{\partial}{\partial\phi} = \frac{2}{\Delta\Phi}\frac{\partial}{\partial\xi} \tag{6}$$

$$\frac{\partial}{\partial\lambda} = \frac{2}{\Delta\Lambda}\frac{\partial}{\partial\eta} \tag{7}$$

The leading terms of thick-plate strain at depth z reckoned from a neutral layer $z = 0$ are dependent on the vertical displacement

$$\epsilon_{\phi\phi}^{(TP)} = -\frac{z}{R^2}\left(\frac{\partial^2 u}{\partial\phi^2} - \nu\frac{1}{\sin^2\phi}\frac{\partial^2 u}{\partial\lambda^2}\right) \tag{8}$$

$$\epsilon_{\lambda\lambda}^{(TP)} = -\frac{z}{R^2}\left(\frac{1}{\sin^2\phi}\frac{\partial^2 u}{\partial\lambda^2} - \nu\frac{\partial^2 u}{\partial\phi^2}\right) \tag{9}$$

$$\epsilon_{\phi\lambda}^{(TP)} = -\frac{z}{R^2\sin\phi}\frac{\partial^2 u}{\partial\phi\partial\lambda} \tag{10}$$

with the Poisson ratio ν. The Chebyshev expansion of the surface displacements and with it the strain is supposed to include the

Table 1
Results of observation fit. We show the weighted RMS of signal and residual of all sites and the maximum error in each component. The maximum WRMS over the three components per station is shown in bold.

Input	WRMS all sites		Maximum WRMS site	Maximum error [mm/yr] $\pm 1\sigma$	Comp.	Site
	Signal	Residual				
Thick plate						
GPS	15.3	0.78	**2.7**	0.50 ± 0.12	E	SUUR
			0.67	1.36 ± 1.5	U	BORK
			0.58	0.79 ± 0.95	N	SMID
			0.58	0.53 ± 1.0	E	SMID
Model	12.6	0.07	**0.22**	0.008 ± 0.05	N	KIVE
			0.16	0.12 ± 0.4	U	BODS
			0.10	0.018 ± 0.07	N	OSLS
			0.01	0.025 ± 0.5	E	BORK
Model−GPS	4.5	0.90	**3.29**	0.61 ± 0.12	E	SUUR
			0.75	1.17 ± 1.5	U	BORK
			0.53	0.38 ± 0.95	N	SMID
			0.53	0.71 ± 1.0	E	SMID
Thin plate						
GPS	15.3	0.79	**3.4**	0.64 ± 0.12	E	SUUR
			0.60	1.22 ± 2.0	U	SMID
			0.84	0.54 ± 0.6	N	BORK
			0.60	0.77 ± 1.0	E	SMID
Model	12.6	0.04	**0.10**	0.012 ± 0.08	N	MAR6
			0.01	0.050 ± 2.0	U	SMID
			0.06	0.026 ± 0.26	N	SASS
			0.1	0.023 ± 1.4	E	OSLS
Model−GPS	4.5	0.78	**3.45**	0.64 ± 0.12	E	SUUR
			0.52	1.02 ± 2.0	U	SMID
			0.54	0.39 ± 0.6	N	BORK
			0.52	0.64 ± 1.0	E	SMID

thick-plate action. Thus, the strain at depth z becomes

$$\epsilon(z) = \epsilon^{(S)} - \epsilon^{(TP)}(z)$$

for any horizontal component, superscript S denoting the surface strain (Eqs. (2)–(5)).

The penalty function is formulated as follows:

$$P = \frac{1}{N_{\text{obs}}} \sum_{i=1}^{N_{\text{obs}}} (\tilde{\mathbf{u}}_i - \mathbf{u}_i)^\top \cdot \boldsymbol{\sigma}^{-2} \cdot (\tilde{\mathbf{u}}_i - \mathbf{u}_i)$$
$$+ \frac{\Omega}{N_e} \sum_{i=1}^{N_e} [E(\phi_i, \lambda_i) + B(\phi_i, \lambda_i)] \tag{11}$$

where the first term computes the normalised χ^2 of the fit of observations $\tilde{\mathbf{u}}_i$, the second term the elastic and the third the buoyancy energy. Each observation error is scaled with its standard deviation. The energy terms are scaled with Ω, the energy penalty factor. E consists of the in-plane and bending strain energy density (in N/m)

$$E = \frac{1}{2} \int_{-T_l/2}^{T_l/2} \left[\boldsymbol{\sigma} : \boldsymbol{\epsilon} + \boldsymbol{\sigma}^{(TP)}(z) : \boldsymbol{\epsilon}^{(TP)}(z) \right] \, \mathrm{d}z \tag{12}$$

and buoyancy energy density

$$B = \frac{1}{2} g \rho_{\text{eff}} u^2 \tag{13}$$

sampled at N_e random points. The stress tensor $\boldsymbol{\sigma}$ is obtained from the strain tensor $\boldsymbol{\epsilon}$ by means of the Hooke–Lamé equations, and the colon signifies the dyadic product.

Finally, we search for a minimum of P by varying the Chebyshev coefficients in the matrix $\mathbf{U}$. Since all equations are linear in the coefficients, the partial derivatives of P can easily be computed from the difference of P switching each coefficient between unity and zero.

The uncertainties for the estimated quantities are computed only with respect to the observation fit, the first term in (11). Varying each Chebyshev-coefficient we obtain a normalised χ^2 that is larger than the best fit value. We invert the equation to determine the range of variation such that the observation square-error is enlarged by a factor of 2, spreading the individual contributions equally. While stepping through a regular longitude–latitude grid, the RMS of the deviations in each target quantity is summed up. Thus we obtain the RMS of all deviations (e.g. of areal strain rate) that in its entirety leads to a half-as-good observation fit.

Here's the method. Let $\mathbf{1}_{ijk}$ be a zero matrix except for a value of unity at ijk. Let further $q(\phi, \lambda, \mathbf{U})$ be a target quantity (e.g. areal strain) with $\boldsymbol{U^*}$ the $M \times N \times 3$ matrix of Chebyshev-coefficients pertaining to the best fit. Denote the observation penalty by χ^2. Assume that varying coefficient ijk by $\delta U_{ij}^{(k)}$ creates an increase of χ^2 by $\delta\chi^2$.

$$\chi^2(\boldsymbol{U^*} + \mathbf{1}_{ijk}\delta U_{ij}^{\pm(k)}) - \chi^2(\boldsymbol{U^*}) = \delta\chi^2 \tag{14}$$

To obtain a value for $\delta U_{ij}^{\pm(k)}$ we demand that

$$\delta\chi^2 = \alpha \frac{\chi^2(\boldsymbol{U^*})}{3MN} \tag{15}$$

$\alpha = 1$ for a doubling of the misfit. Eq. (14) is solved iteratively a root finder. Finally

$$\sigma = \sqrt{\frac{1}{2} \sum_{ijk\pm} \left[q(\phi, \lambda, \boldsymbol{U^*} + \mathbf{1}_{ijk}\delta U_{ij}^{\pm(k)}) - q(\phi, \lambda, \boldsymbol{U^*}) \right]^2} \tag{16}$$

is our estimate of the uncertainty of q at ϕ, λ.

3. Data

The study will be carried out on two kinds of input data. First we use GIA model predictions (Milne et al., 2004) in order to supply a well known signal. At this stage we can analyse how well the
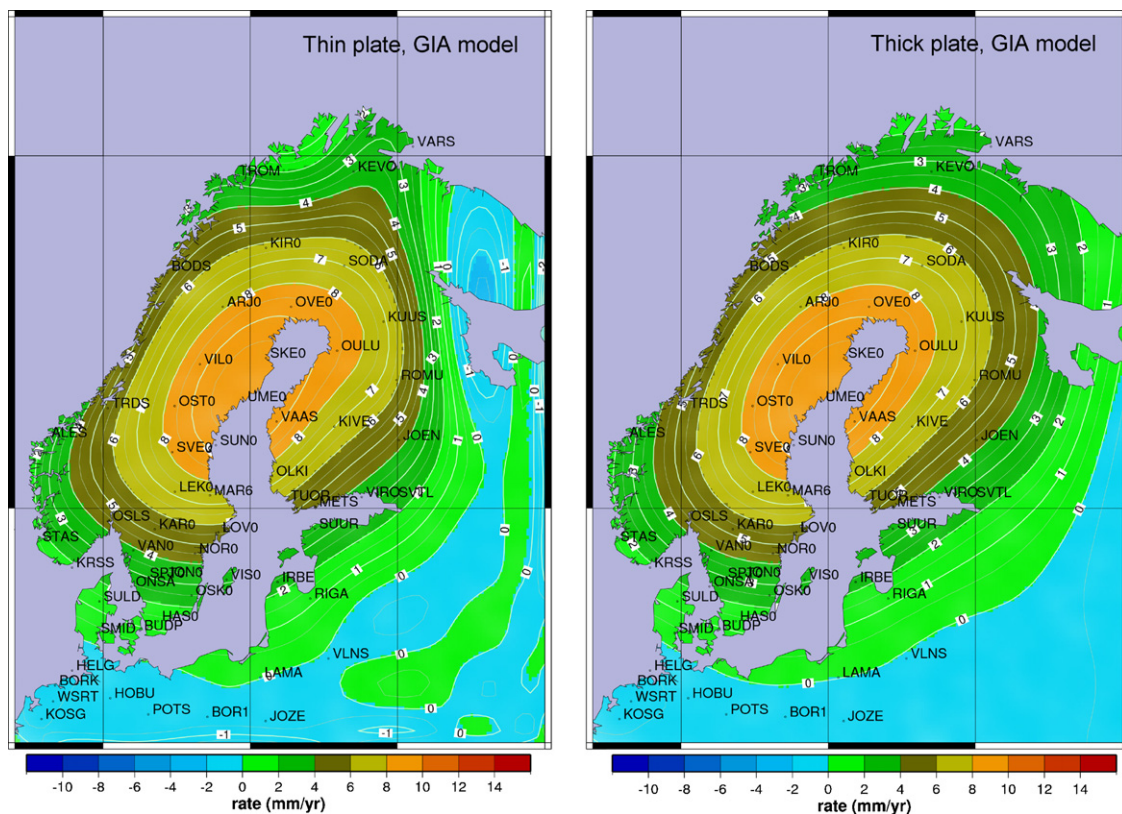
Fig. 1. Vertical rates modelled with a thin plate (left) and a thick plate (right). The data fitted are the GIA predictions from Milne et al. (2004).
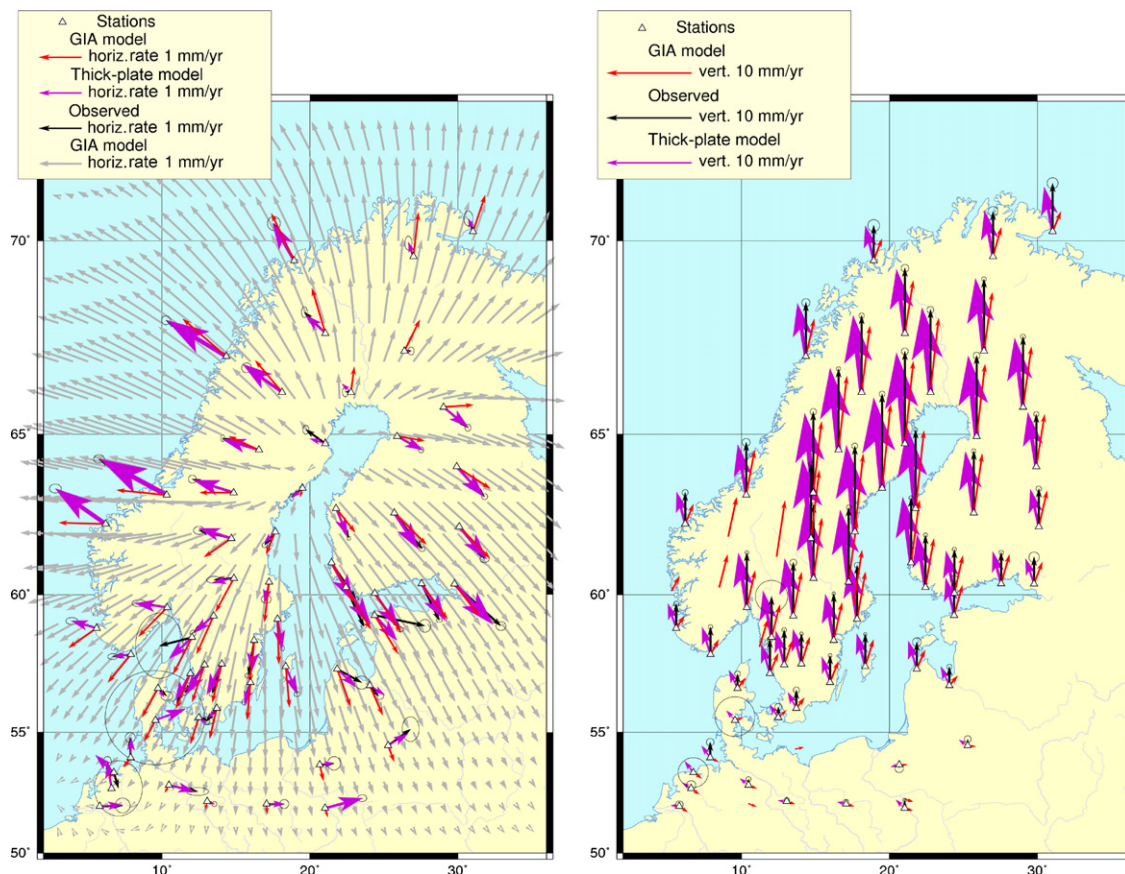
Fig. 2. Displacement rates. Observed GPS solution from Lidberg et al. (2010), GIA predictions from Milne et al. (2004) and the fit to the GPS data using a thick elastic plate.
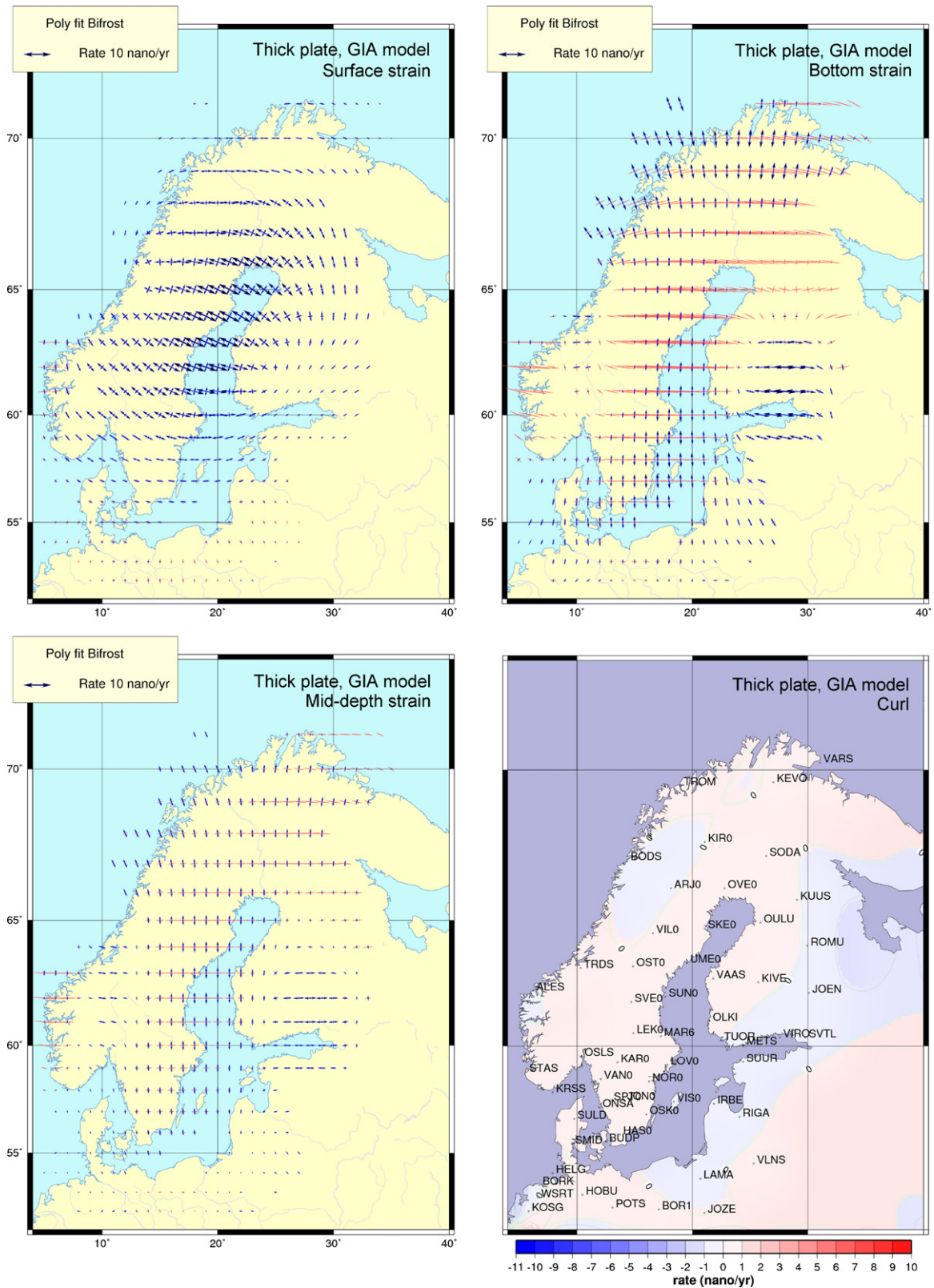
Fig. 3. Strain rates computed by the thick-plate model at surface and bottom of the slab (top row) and at mid-plane depth (bottom left). Curl is show in the bottom right map.

discrete GNSS station network can retrieve the continuous field. The particular model selected has a lithosphere thickness of 120 km, an upper mantle viscosity of 0.5×10^{21} Pa s and a lower mantle viscosity of 5×10^{21} Pa s.

This model provided the best fit to the GPS solution of Lidberg et al. (2010). It should be noted that the vertical velocities produced by the GIA model are in general somewhat lower; however, the fit to the 3-D motions did prefer this model probably because the
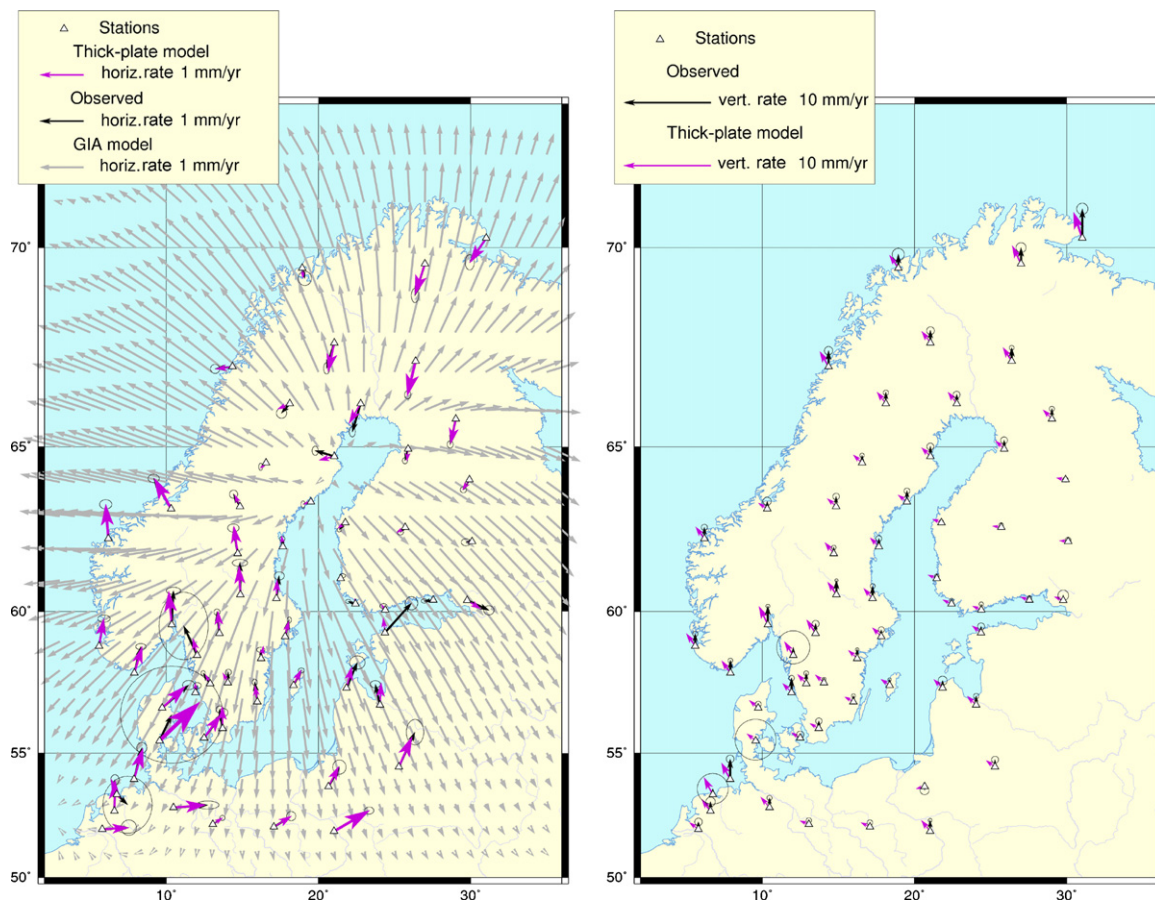
Fig. 4. Residual motion (GPS minus GIA model), horizontal velocities left, vertical right, and the thick-plate solution.

northward velocities in the north are generally overpredicted by the suite of models, maybe as a consequence of an ice load not extending sufficiently into the Barents area. Therefore, a generally lower velocity scale has advantages in the fit.

Since GIA produces an uplift dome with large vertical rates we will also study the importance of thick-plate flexure for the horizontal strain rates at the surface. In a second stage we adjust the thick-plate model to the difference between model and BIFROST GNSS site velocities.

As the observation data set we use the GPS solution of Lidberg et al. (2010). The thick-plate model is adjusted to the difference of the GIA model velocities minus those of the GPS solution.

4. Results and discussion

The following computations will be examined more closely: (1) The response of the thin- and thick-plate models to the GIA model predictions at the GNSS stations along with the uncertainty of the GNSS observations. (2) The difference of the GNSS observations and the GIA model predictions. Table 1 summarises the success of the adjustments along with the maximum residual errors. The table also shows one run of the model where the GPS solution is fitted before subtracting the GIA predictions.

Graphics for the resulting uncertainties of inferred strain components cannot be shown here because of space limitations. In short, the areal and shear strain uncertainties are typically on the order of 1×10^{-9}/yr in the areal component, 2×10^{-9}/yr in shear, and 0.5 nrad/yr in curl. The uncertainties become five times larger

towards the edges of the model. These particular numbers apply to fit of the thick plate to the residual motion.

4.1. Fit to the GIA model predictions

Both the thin- and thick-plate models can be fit to the GIA predictions with a weighted residual RMS much less than unity. The thick-plate penalty due to flexure is seen to smoothen the response in the thick-plate solution, reproducing more closely the features of the GIA model as seen in Milne et al. (2004) (cf. Fig. 1).

We show the deformation field in Fig. 2 where the thick-plate adjustment can be compared to the input GIA field.

The thin- and thick-plate solutions differ significantly as to the amount of in-plane strain at depth. Assuming a 200 km thickness of the slab, the flexure is found to contribute to horizontal surface displacement at a magnitude three to four times with respect to observations or GIA predictions. Each extension due to flexure around one axis is accompanied by a compression at right-angle and scaled with the Poisson ratio. Thus the already smaller NE–SW extension is reduced further due to sharper bending around the NE–SW flexure axis. As a consequence, the mid-plane areal strain and the NW-SE strain component switch sign from extensional to compressional in the thick plate. As a further consequence the displacements at the bottom of the slab become inward-directed at magnitudes of 5 mm/yr. Strain at the three depth levels is shown in Fig. 3.

Stepping beyond this simple model and contemplating the situation of viscous coupling of the asthenosphere when the isostatic rebound is in a phase of relaxation, the corresponding stress change would act in an opposite sense, extending the lithosphere rather
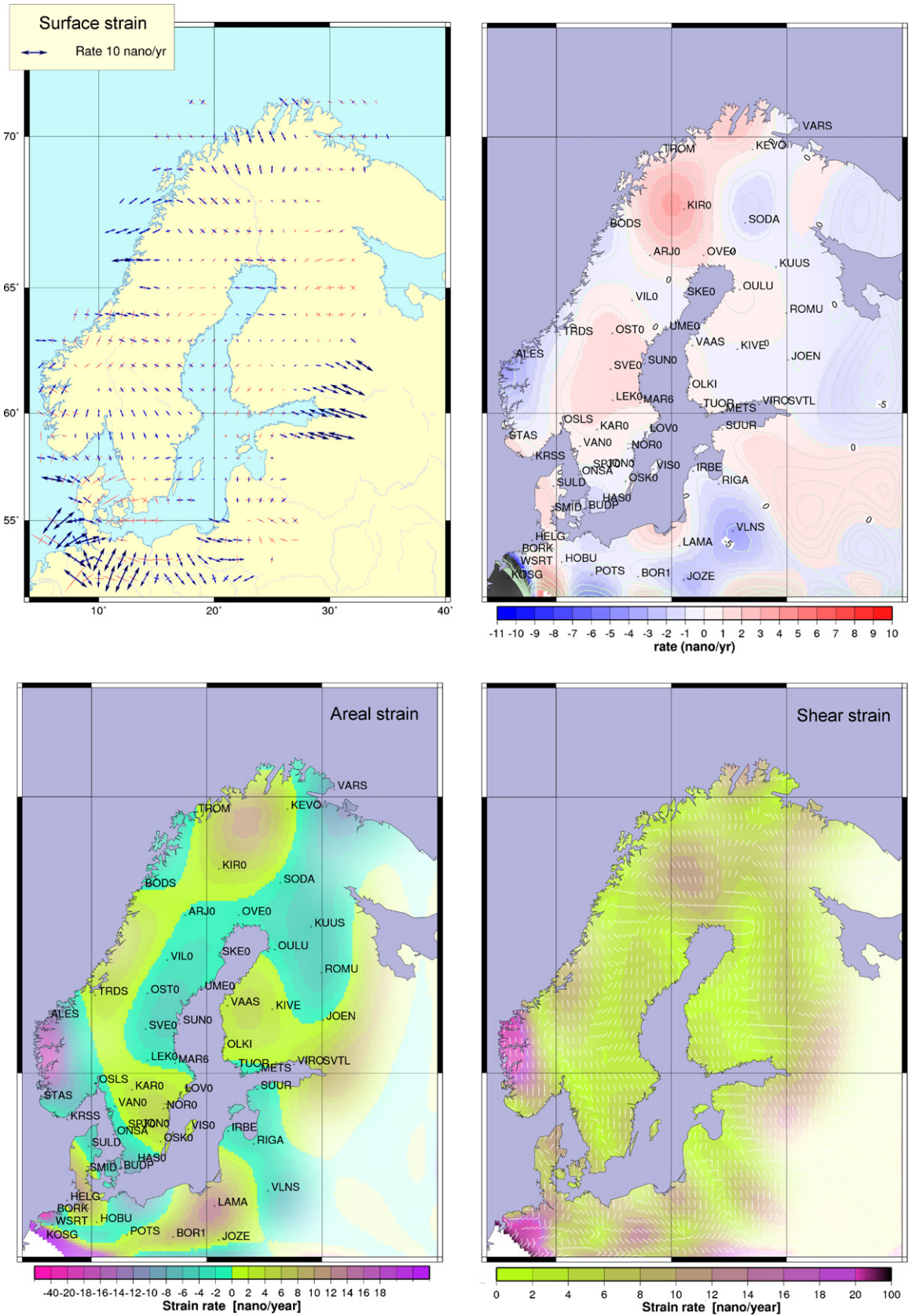
Fig. 5. Thick-plate solution for surface strain rates (left) and curl (right) derived from the residual observed motion after subtracting the GIA predictions.

than compressing. If the thick-plate model is correct the flexing lithosphere would increase the stress at the boundary to the asthenosphere. This would lead to increased compression in the lower lithosphere and a downward shift of the neutral layer, and thus an increased extension at the surface in excess to what is computed in our thick-plate model that assumed horizontal stress-free conditions at the bottom of the slab. A more realistic vertical profile of horizontal stress in the lithosphere must be left to future development of the model.

The GIA predictions are based on a set of spheroidal base functions, and for that reason curl in the displacement field is zero. The "filtering" of the field through the GNSS network and its weighting produces a curl field that is in general less than the estimated uncertainty (cf. Fig. 3).

4.2. Fit to the observed GIA model residual

Two sites were reweighted owing to short records, assuming the long-term noise has not been averaged to the same level as in the longer records: SMID in Denmark and BORK on the North Sea island of Borkum, Germany. No further efforts have been taken to perform robustness tests or reweighting of some of the observations in the fit as the majority of WRMS contributions is near unity or below.

Examining the results of the plate models when they are fitted to the residual observations (GNSS minus GIA-model, see Fig. 4) we emphasize the following features. In the northern part of the area the GIA model overpredicts the observed horizontal motion. To some extent this is a consequence of the sparseness of the GNSS network. With more stations in the north the minimisation of the misfit would have distributed the residual more evenly over the region, since there are three degrees of freedom in the GNSS results with respect to the origin of global rotation. However, since the plate model is formulated in a spherical geometry, and since it has free-slip boundaries, we can rely on the absorption of a rigid rotation in the curl of the displacement field.

Fig. 5 shows the thick-plate solution for surface strain and curl. Strain is also shown in the areal and shear components. The negative areal strain rates found throughout the central and northern parts of Fennoscandia suggests that the GIA model overpredicts the GPS results primarily in the aspect of areal strain.

One conspicuous feature is found north of Kiruna. It appears that the station rate of Tromso is relatively large towards the north. The thick plate responds by a pair of curl centres with clockwise rotation towards the east and counter-clockwise towards the west while compression turns over to extension in between the curl dipole. Also shear strain obtains a local maximum there. The area is one of the least well-resolved regions in the GNSS network. The question that arises, whether the horizontal motion of Tromsö is an extended phenomenon, would require at least two additional observing sites in Finnmarken. A similar wish is expressed regarding the south-western Norwegian highland and fjords area.

Another noteworthy feature in an area well covered by the GNSS network is found in southwest Finland and in southern Sweden, where GIA rates underpredict the GPS velocities, and consequently a region of extension is detected. The highest strain rates are found either along the edges of the GNSS station network or in the region covering Belgium, the Netherlands, Northern Germany, Denmark and Poland. With respect to the uneven quality of station monumentation, ground coupling, length of time series in the latter areas we hesitate to conclude strong indications of localised crustal deformation.

5. Conclusions

We have obtained first results of strain rate determination from a GPS velocity solution by adjusting an elastic, thick plate in a simultaneous minimisation of elastic and potential energy, and observation misfit. One conclusion that appears important and safe is that flexure is an important contributor to the strain rates and their style in the plate, particularly at depth.

Analysing the part of the observed motion that remains unexplained using a best fitting model for glacial isostatic adjustment (GIA) we find conspicuous features in the strain rate field in areas where the station network is sparse. In most of the rebound area, however, residual strain rates are on the order of up to 7 nano/yr. The central area, where glacial isostatic adjustment is prevailing, shows uniform strain rates; the data does not support the notion of lateral shear exceeding 4 nano/yr. Two regions are identified where strain rates are either under- or overpredicted by a GIA model, underprediction in the central and northern uplift area und overprediction in southern Finland and Sweden.

Curl is confined to a range of ± 2 nrad/yr except in northern Finland and Finnmarken. In this area, also strain rate maxima are found. However, owing to the sparseness of the GNSS network in the north and west, the impact of anomalous motion at the few sites in the topographic slope in the fjord regions of the Scandian mountain belt is high and more definite conclusions as to a complex deformation pattern in northern Sweden and Findland would require more observing sites.

References

Cai, J., Grafarend, E.W., 2007. Statistical analysis of geodetic deformation (strain rate) from the space geodetic measurements of BIFROST Project in Fennoscandia. J. Geodyn. 43, 214–238.

Haas, R., Scherneck, H.-G., Gueguen, E., Nothnagel, A., Campbell, J., 2002. Large-scale strain-rates in Europe derived from observations in the European geodetic VLBI network. EGU Stephan Mueller Spec. Publ. Ser. 2, 1–14.

Lidberg, M., Johansson, J.M., Scherneck, H.-G., Davis, J.L., 2006. An improved and extended GPS-derived 3-D velocity field of the glacial isostatic adjustment (GIA) in Fennoscandia. J. Geodesy 81, 213–230.

Lidberg, M., Johansson, J.M., Scherneck, H.-G., Milne, G.A., 2010. Recent results based on continuous GPS observations of the GIA process in Fennoscandia from BIFROST. J. Geodyn. 50, 8–18.

Milne, G.A., Mitrovica, J.X., Scherneck, H.-G., Davis, J.L., Johansson, J. M., Koivula, H., Vermeer, M., 2004. Continuous GPS measurements of postglacial adjustment in Fennoscandia: 2. Modeling results. J. Geophys. Res., 109, doi:10.1029/2003JB002619.

Nocquet, J.-M., Calais, E., Parsons, B., 2005. Geodetic constraints on glacial isostatic adjustment in Europe. Geophys. Res. Letters, 32, doi:10.1029/2004GL022174.

Nyst, M., Thatcher, W., 2004. New constraints on the active tectonic deformation of the Aegean. J. Gephys. Res., 109, doi:10.1029/2003JB002830.

Spakman, W., Nyst, M.C.J., 2002. Inversion of relative motion data for estimates of the velocity gradient field and fault slip. Earth Planet. Sci. Lett. 203, 577–591.

Weisstein, E., (s.d.). http://mathworld.wolfram.com/ChristoffelSymboloftheSecondKind.html.